High Temperature, Vol. 37, No. 6, 1999, pp. 887–894. Translated from *Teplofizika Vysokikh Temperatur*, Vol. 37, No. 6, 1999, pp. 920–927.

HEAT AND MASS TRANSFER AND PHYSICAL GASDYNAMICS

Assessment of the Capabilities of Explicit Algebraic Reynolds Stress Models as Applied to the Calculation of Wall Turbulent Boundary Layers

A. V. Garbaruk, Yu. V. Lapin, and M. Kh. Strelets

St. Petersburg State Technical University, St. Petersburg, 195251 Russia

Received September 2, 1998

Abstract—An explicit algebraic Reynolds stress model (EARSM) is used to perform calculations of canonical turbulent boundary layers on a flat plate under conditions of zero, adverse, and accelerating pressure gradients. A comparison of the results with the calculation data obtained using the standard K–ω and K–ε models of turbulence and with the known experimental data demonstrates that, in spite of the obvious advantages of the EARSM over the traditional models in calculating flows with substantial anisotropy of Reynolds stresses, these advantages, as applied to the class of flows being treated, show up mainly in determining the pulsation parameters of flow. Further, the accuracy of the EARSM in all cases depends strongly on the choice of the base model: from this standpoint, the K–ω model is superior to the K–ε model. The results of calculations of flow past a flat plate demonstrate the need for a more thorough calibration of the EARSM along with the base model.

INTRODUCTION

Since their inception (early 1970s), the differential models of Reynolds stress transfer (DRSM) are treated as a promising alternative to traditional models of turbulence based on the concept of scalar turbulent viscosity (Boussinesq's gradient hypothesis). Nevertheless, no convincing proof of the real superiority of the DRSM over the traditional models has yet been found. At least in part, this is associated with the fact that their use in calculation of fairly complex flows (for the investigation of which the DRSM are primarily intended) involves serious computational difficulties. That is why the development of the relevant algebraic models (ARSM), of which the first was suggested by Rodi [1], was started almost simultaneously with that of the DRSM. The practical experience in using the ARSM has demonstrated that they also suffer from serious disadvantages analyzed in detail in a recent paper by Speziale [2]. In particular, as a result of considerable nonlinearity of model algebraic equations, they fail to guarantee the uniqueness of solution. Moreover, the ARSMs sometimes fail to satisfy the "principle of realizability" formulated by Lumley [3],

$$\overline{u_i'^2} \geq 0, \quad \overline{u_i'^2}\,\overline{u_j'^2} \geq (\overline{u_i'u_j'})^2, \quad \det\{\langle \overline{u_i'u_j'} \rangle\} \geq 0,$$

where $\overline{u_i'u_j'}$ are components of the Reynolds stress tensor, and, under some conditions, prove to be singular, this leading to obvious computational problems.

The above-identified shortcomings of ARSM stimulated the attempts at developing the so-called explicit algebraic Reynolds stress models (EARSM) in which the input model equations are explicitly resolved in one way or another relative to Reynolds stresses, which enables one to attain the uniqueness of solution and simplify the verification of validity of the principle of realizability. In recent years, several models of this type were suggested (see, for example, [4–7]), which were used to calculate fairly complex turbulent flows. For example, as demonstrated by Wallin and Johansson [4], the EARSM they suggested provides an adequately exact calculation of steady-state turbulent flow in a round pipe rotating about its axis. This flow is characterized by the presence of substantial anisotropy of Reynolds stresses, which leads to an appreciable nonlinearity of the profile of tangential component of velocity (this effect in principle cannot be described within the turbulence models based on the concept of scalar turbulent viscosity). Therefore, from this standpoint, the EARSMs exhibit obvious advantages over traditional "isotropic" models and, from the standpoint of computational efficiency, are superior to the classical ARSM, which leads one to treat the development of models of this group and the investigation of their capabilities as one of the most important aspects of the semiempirical theory of turbulence [2]. In view of this, it is of some interest whether the EARSMs provide adequate accuracy in calculating canonical wall flows in which the anisotropy of Reynolds stresses is not of great importance, but which may exhibit some other effects that are difficult to simulate. It is the objective of the present study to provide an answer to this question in application to turbulent boundary layers on flat surfaces.

0018-151X/99/3706-0887$22.00

MODEL OF TURBULENCE

The calculations were performed using the EARSM suggested by Wallin and Johansson [4]. In the general case of an arbitrary plane flow, this model reduces to the following relation for the components of the anisotropy tensor of Reynolds stresses:

$$a_{ij} = \frac{\overline{u_i' u_j'}}{K} - \frac{2}{3} = f_1 \beta_1 S_{ij}$$

$$+ (1 - f_1^2) \frac{3B_2 - 4}{\max(\Pi_S, \Pi_S^{eq})} \left(S_{ik} S_{kj} - \frac{1}{3} \Pi_S \right) \qquad (1)$$

$$+ \left(f_1^2 \beta_4 - (1 - f_1^2) \frac{B_2}{2\max(\Pi_S, \Pi_S^{eq})} \right) (S_{ik} \Omega_{kj} - \Omega_{ik} S_{kj}).$$

Here, $S_{ij} = \frac{\tau}{2}\left(\frac{\partial U_i}{\partial x_j} + \frac{\partial U_j}{\partial x_i}\right)$ and $\Omega_{ij} = \frac{\tau}{2}\left(\frac{\partial U_i}{\partial x_j} - \frac{\partial U_j}{\partial x_i}\right)$ are the components of dimensionless tensors of the rates of deformation and vorticity, $\Pi_S = S_{ij} S_{ji}$ and $\Pi_\Omega = \Omega_{ij} \Omega_{ji}$ are second invariants of the respective tensors, τ is the time scale of turbulence, and K is the kinetic energy of turbulence.

The parameters β_1 and β_4 entering equation (1) are defined by the relations

$$\beta_1 = -\frac{6}{5} \frac{N}{N^2 - 2\Pi_\Omega}, \quad \beta_4 = -\frac{6}{5} \frac{1}{N^2 - 2\Pi_\Omega},$$

where N is the solution of the following cubic equation:

$$N^3 - C_1' N^2 - (2.7\Pi_S + 2\Pi_\Omega) N + 2C_1' \Pi_\Omega = 0.$$

This solution may be represented as

$$N = \frac{C_1'}{3} + (P_1 + \sqrt{P_2})^{1/3}$$

$$+ \operatorname{sgn}(P_1 - \sqrt{P_2}) \left| P_1 - \sqrt{P_2} \right|^{1/3} \quad \text{for} \quad P_2 \geq 0,$$

$$N = \frac{C_1'}{3} + 2(P_1^2 - P_2)^{1/6}$$

$$\times \cos\left(\frac{1}{3} \arccos\left(\frac{P_1}{\sqrt{P_1^2 - P_2}} \right) \right) \quad \text{for} \quad P_2 < 0,$$

$$P_1 = \left(\frac{C_1'}{27} + \frac{9}{20} \Pi_S - \frac{2}{3} \Pi_\Omega \right) C_1',$$

$$P_2 = P_1^2 - \left(\frac{C_1'}{9} + \frac{9}{10} \Pi_S + \frac{2}{3} \Pi_\Omega \right).$$

The empirical damping function f_1 introduced into the model to include the wall effects is defined as $f_1 = 1 - \exp(-y^+/A^+)$. The empirical constants of the model, obtained by Wallin and Johansson [4, 5] from the comparison of the calculation results with the experimental data and data of direct numerical simulation [8] by the steady-state flow in a flat channel, are

$$C_1' = 2.25(C_1 - 1), \quad C_1 = 1.8, \quad B_2 = 1.8, \quad A^+ = 26,$$

$$\Pi_S^{eq} = \frac{405 C_1^2}{216 C_1 - 160}.$$

For the case of turbulent boundary layer on a flat surface, the equation of motion contains only one component of Reynolds stress tensor $\overline{u'v'}$. It can be readily demonstrated that the following relation may be derived in the boundary layer approximation from the general expression (1) for this component:

$$\overline{u'v'} = \frac{f_1 \beta_1 K \tau}{2} \frac{\partial U}{\partial y}, \qquad (2)$$

which enables one to introduce the turbulent viscosity determined by the formula

$$\nu_t = -\frac{f_1 \beta_1 K \tau}{2}. \qquad (3)$$

In order to close model (1), as any other ARSM, one must add relations for determining the kinetic energy K and for the time scale τ of turbulence. These relations provide a basis for the respective ARSM and represent an important part of the complete model.

In our study, we use the modifications of the K–ε model of Chien [9] and K–ω model of Wilcox [10], which were specially suggested by Wallin and Johansson [4]. The difference of the employed version of the Chien model from its original version consists in that the correlation between the true and modified rates of dissipation of turbulence is defined by the relation $\varepsilon = \tilde{\varepsilon} + 2\nu K/y^2 \exp(-C_k y^+)$ with the constant $C_k = 0.04$, rather than by the relation $\varepsilon = \tilde{\varepsilon} + 2\nu K/y^2$. In the K–ω model of Wilcox, use is made of the following value of one of its empirical constants: $R_\beta = 10$ (instead of eight in the original model). In so doing, it is assumed in both cases that the turbulent viscosity appearing in the transport equations for K, ε, and ω of the respective models is determined by formula (3).

After K and ε or K and ω are found, the time scale of turbulence is defined either as $\tau = \max(K/\varepsilon, 6\sqrt{\nu/\varepsilon})$ [11] or as $\tau = \max((\beta^* \omega)^{-1}, 6\sqrt{\nu/(\beta^* \omega K)})$, where β^* is the empirical function of Wilcox' model [10], which allows for the wall effects.

For numerical integration of the system of boundary layer equations, a two-layer implicit difference scheme of the Crank–Nicholson type was used, which had the first order of approximation on the longitudinal coordinate and the second order of approximation on the transverse coordinate. In so doing, the boundary layer on a flat plate was calculated by the traditional direct method of solving the boundary layer equations, in

which the longitudinal distribution of velocity was preassigned as the boundary conditions on the external boundary. The inverse method [12, 13] was used to calculate boundary layers with a pressure gradient, in which the velocity along the external boundary was determined by the preassigned distribution of the boundary layer displacement thickness.

The no-slip and impermeability conditions were used as the boundary conditions for velocity on the wall. The quantities K and ε on the wall were taken to be zero, and the specific rate of dissipation ω was determined, in accordance with [14], by the formula $\omega = 60\nu/(\beta\Delta y^2)$, where $\beta = 0.075$ and Δy is the wall mesh width.

When the K–ε model was used as basic, the values of K and ε were preassigned on the external boundary. It was assumed that K was equal to $10^{-3}U_e^2$, which corresponded to a low degree of turbulence of incident flow in the experiments for which the calculations were made, and ε was determined by the preassigned turbulent viscosity ($\nu_t = 10^{-3}\nu$) using the formula $\varepsilon = 0.09K^2/\nu_t$. When the K–ω model was used as basic, the value of K was preassigned analogously, and the value of ω was calculated by the formula $\omega = 4\tau_W/\rho/(\beta^{*1/2}U_e\delta^*)$ [14], where τ_W is the wall friction, ρ is the density, U_e is the velocity on the external boundary of the boundary layer, and δ^* is the displacement thickness.

The profiles of the longitudinal component of velocity and of the respective turbulent characteristics (K and ε or K and ω) were preassigned in the initial cross section of the boundary layer.

The calculations were performed in a nonuniform (crowding of points in the vicinity of the wall) net with respect to y. The ratio between the neighboring mesh widths did not exceed 1.05, and the wall mesh width was selected such that the condition $y^+ < 0.1$ would be valid in the first node after the wall.

DISCUSSION OF THE RESULTS

The known experimental results available from the database of Stanford University were used as tests for assessing the capabilities of the EARSM being treated in calculating plane turbulent boundary layers. In particular, the boundary layer on a flat plate (experiment 1400 [15]) was treated, as well as boundary layers with accelerating (experiment 2700 [15]) and adverse (experiments 0141 [16] and 4800 [15]) pressure gradients. The results obtained within the EARSM using the above-described modifications of the K–ε model of Chien and of the K–ω model of Wilcox (EARSM-CH and EARSM-WL, respectively) were compared with the results of calculations within the original models of Chien [9] (CH) and Wilcox [10] (WL).

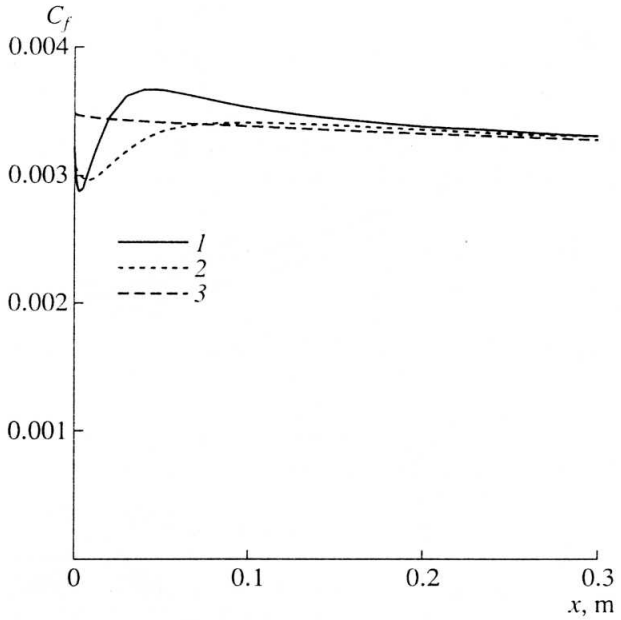

Fig. 1. The effect of the initial conditions on the calculated distribution of the friction coefficient in experiment 4800 using the EARSM-CH model: (*1*) inlet profiles are calculated using the CH model, (*2*) EARSM-WL model, (*3*) EARSM-CH model.

Unfortunately, the above-identified experimental results do not include experimental data on the turbulent characteristics of flow in the initial cross section of the boundary layers being treated, which are required for preassigning the initial conditions for the respective transport equations. With a view to determining these characteristics, the calculation of each one of the treated flows using each model was preceded by the calculation of the boundary layer on the plate up to the cross section in which the calculated value of the displacement thickness coincided with the respective value in the first experimental cross section (for $x = x_0$). The resultant velocity profiles and turbulent characteristics of flow were used as initial (at $x = x_0$) conditions in performing the main calculation. Obviously, such an approach is approximate; however, as demonstrated by the results of special numerical experiments, in the case when the inlet profiles of velocity and turbulent characteristics agree with one another (i.e., are calculated using one and the same model of turbulence), the uncertainty in their preassignment affects the calculation results only in a relatively small zone which is a minor part of the flow being treated. This is confirmed by Fig. 1, which gives, by way of example, the longitudinal distribution of the friction coefficient for experiment 4800, calculated by the EARSM-CH model using the inlet profiles obtained by the method described above with the aid of the EARSM-CH, CH, and EARSM-WL models. One can see that all curves almost coincide with one another even at $x = 0.2$ m, while the overall extent of the boundary layer in the experiment is more than 5 m.

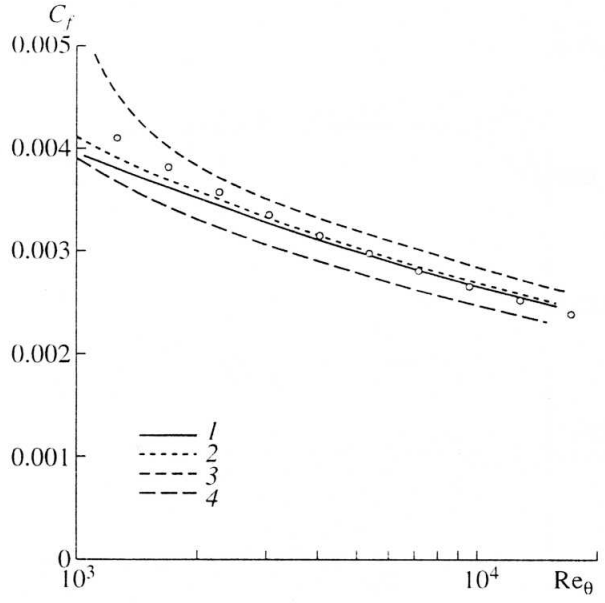

Fig. 2. Comparison of the results of calculation of the friction coefficient on a flat plate with the Bradshaw correlation formula: (*1*) CH model, (*2*) WL model, (*3*) EARSM-CH model, (*4*) EARSM-WL model; the dots indicate the Bradshaw formula.

The results of the main series of calculations are given in Figs. 2–10.

In analyzing these results, note, first of all, the fact that, for the case of boundary layer on a flat plate (experiment 1400, Figs. 2–4), the EARSM irrespective of the employed base is inferior to the original CH and WL models as regards the accuracy of calculation of the averaged flow parameters, in particular, the friction coefficient and velocity profile (Figs. 2, 3a). This result appears quite natural, because the empirical constants and functions in the CH and WL models were determined primarily on the basis of comparison with the experimental data on the averaged characteristics of boundary layer on the plate, and those in the EARSM were based on the results of comparison of the calculation results with the data of direct numerical simulation of flow in a flat channel [4, 5].

In calculating the pulsation characteristics of turbulence, all of the treated models predict close profiles of tangential Reynolds stresses, which are in adequate agreement with the experimental data [17] (Fig. 3c). The profiles of the kinetic energy of turbulence calculated using the WL and CH models differ from each other appreciably (the WL model exhibits an appreciable advantage), while both EARSMs predict close results that agree adequately with experiment (see Fig. 3b).

Also of interest are the profiles of normal components of the Reynolds stress tensor (Fig. 4a), calculated using the EARSMs (relation (1)). One can see that, irrespective of the base employed, the EARSMs produce close and at least qualitatively correct results: in the internal region of the boundary layer, the component $\overline{v'^2}$ proves to be much less than $\overline{u'^2}$. Obviously, this effect cannot be described using the CH and WL models based on the Boussinesq hypothesis according to which these components are equal to each other. Fig. 4b gives the profiles of the function $F = -0.5 f_1 \beta_1$, which, according to (3), is an analog of the function $C_\mu f_\mu$ (C_μ = 0.09 is Kolmogorov's constant) entering most of the semiempirical models of turbulence. One can see from this figure that, irrespective of the base employed, the EARSMs describe qualitatively correctly the behavior of variation of the function F (in the range of validity of the wall law, it proves to be almost constant and close to Kolmogorov's constant of 0.09).

The results of calculation of the boundary layer on a flat plate lead one to conclude that, although the

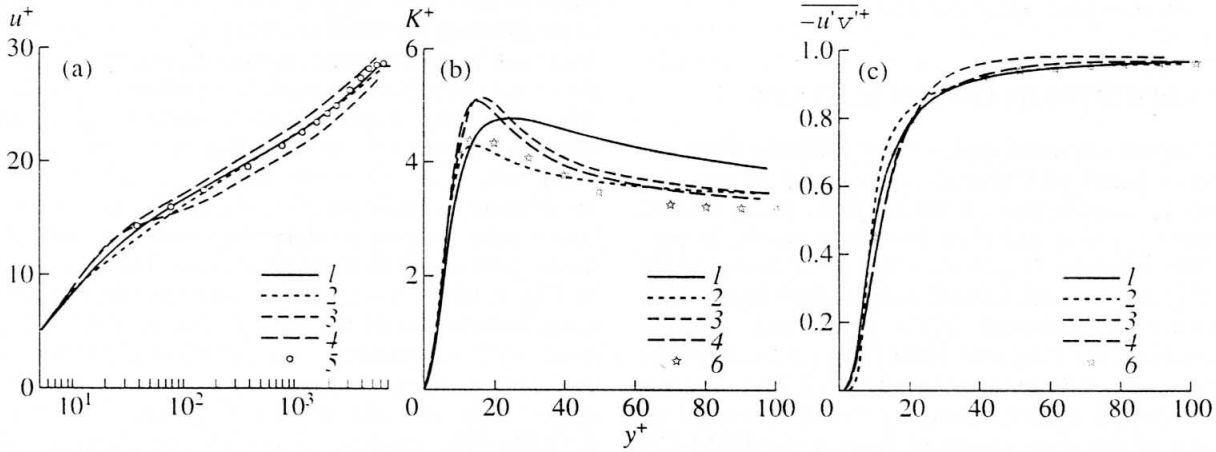

Fig. 3. Comparison of the results of calculation of the profile of (a) velocity, (b) kinetic energy of turbulence, and (c) tangential Reynolds stress with the experimental data on the boundary layer on a flat plate for $x = 4.987$ m: (*1–4*) same as in Fig. 2, (*5*) experimental data of [15], (*6*) experimental data of [17].

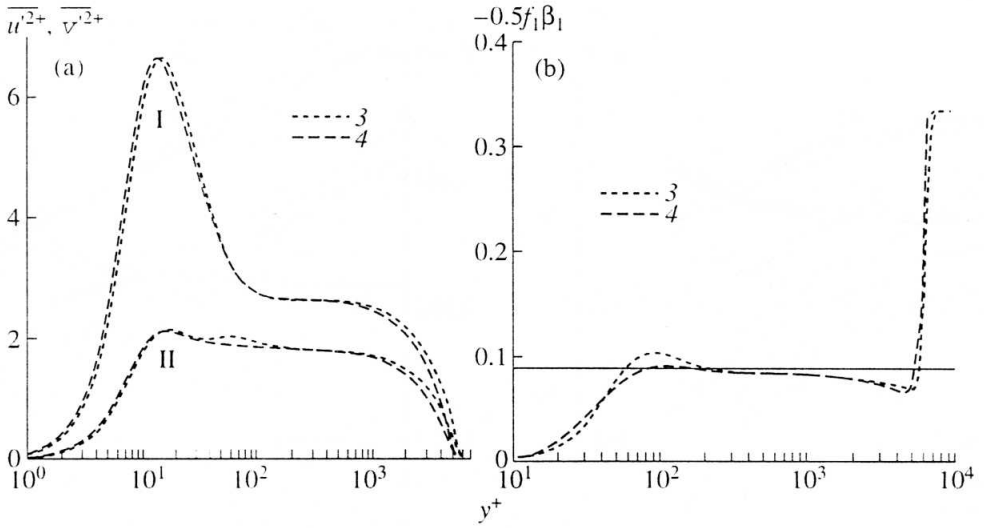

Fig. 4. The profiles of (a) the normal components of the Reynolds stress tensor and (b) the function $-0.5f_1\beta_1$ on a flat plate for x = 4.987 m, calculated using the models (*3*) EARSM-CH and (*4*) EARSM-WL. In Fig. 4a: I—$\overline{u'^2}$, II—$\overline{v'^2}$.

EARSM is somewhat inferior to the original CH and WL models as regards the exactness of calculation of averaged parameters (this disadvantage may apparently be eliminated by refining the model constants), the finer pulsation characteristics of flow are predicted by the EARSM more accurately than by the original models and, for this case, the Wilcox model–based EARSM has some advantage over the Chien model–based EARSM.

We will treat the results of calculation of boundary layers with a pressure gradient.

Figure 5 gives the longitudinal distribution of the main characteristics of the boundary layer for experiment 2700 ($dp/dx < 0$). One can see from this figure that, by and large, this flow is described by all of the models being treated with adequate accuracy. This result is quite predictable, because it is known that the calculation of flows with moderate (not leading to relaminarization of flow) accelerating pressure gradients, as well as the calculation of boundary layer with zero pressure gradient, presents no special difficulties when using almost all of the known models of turbulence.

In view of this, the results of calculation of boundary layers with adverse pressure gradient, given in Figs. 6–10, appear to be of more importance.

An analysis of these results leads to the following conclusions.

First, in this case, the properties of the model used as the base are largely "inherited" by the respective EARSM and essentially define the accuracy of the results. For example, in both treated cases (experiments 0141 and 4800), the EARSM-WL is superior to the EARSM-CH as regards the exactness of calculation of the averaged flow parameters. This is apparently associated with the known disadvantages of the Chien model and other models of the K–ε type in calculating flows with adverse pressure gradient, especially, when approaching the separation point (this defect of the original Chien model is clearly seen in Figs. 6, 7).

Second, unlike the previously treated boundary layers with zero and accelerating pressure gradients, the

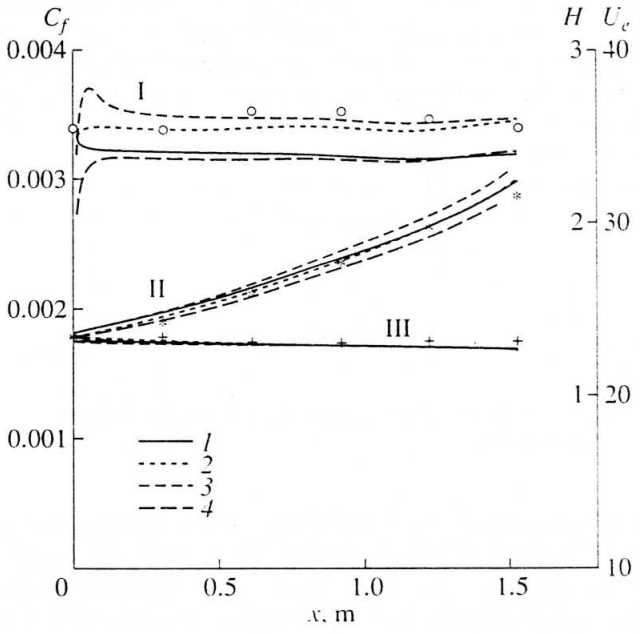

Fig. 5. Comparison of the results of calculation of longitudinal distribution of the main characteristics of boundary layer with the data of experiment 2700: I—friction coefficient C_F, II—form parameter H, III—velocities U_e on the external boundary of the boundary layer; (*1*–*4*) same as in Fig. 2; the dots indicate the experiment.

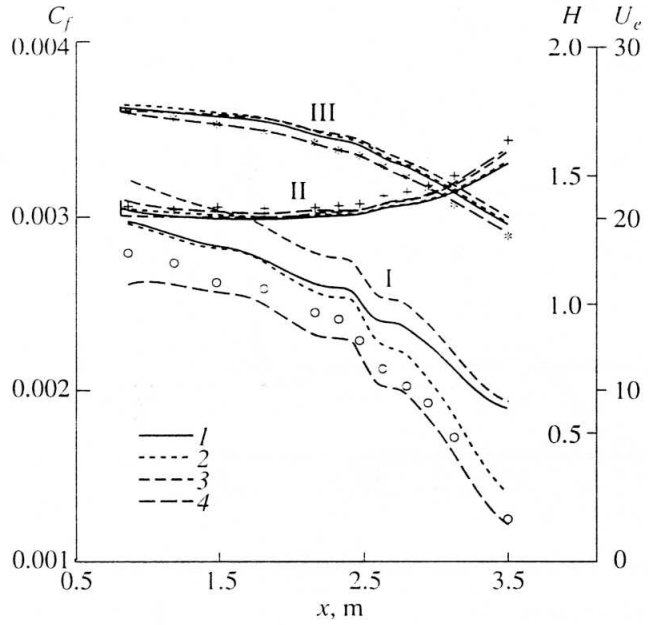

Fig. 6. Comparison of the results of calculation of longitudinal distribution of the main characteristics of boundary layer with the data of experiment 0141. Designations are the same as in Fig. 5.

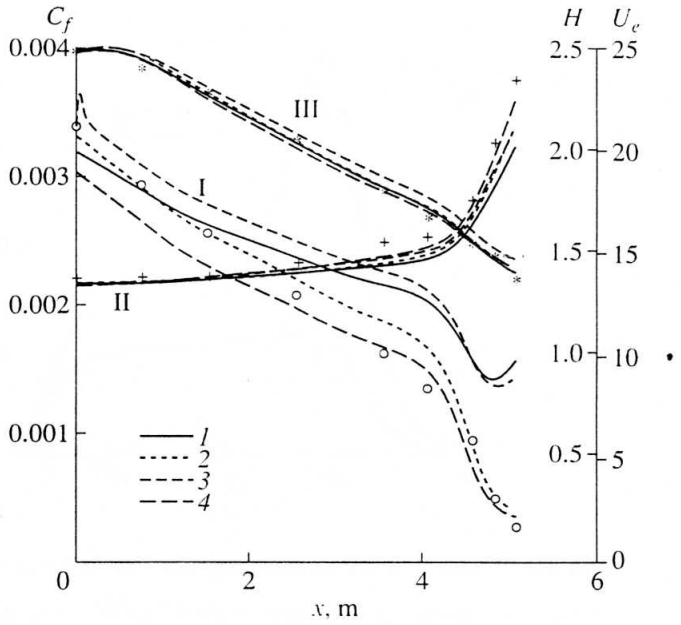

Fig. 7. Comparison of the results of calculation of longitudinal distribution of the main characteristics of boundary layer with the data of experiment 4800. Designations are the same as in Fig. 5.

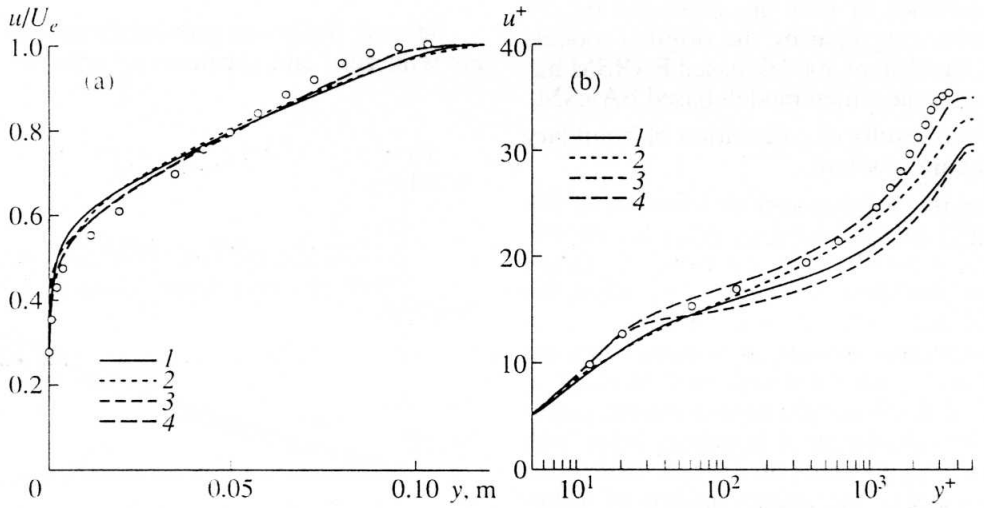

Fig. 8. Comparison of the experimental and calculated velocity profiles in experiment 4800 for x = 3.556 m. Designations are the same as in Fig. 5.

Wilcox model–based EARSM is clearly advantageous over the original Wilcox model. This shows up clearly in comparing the calculated and experimentally obtained profiles of velocity (Figs. 8a, 9a) and pulsation parameters of flow, in particular, the profiles of tangential Reynolds stresses (Fig. 9c). Note that in experiments, in spite of the presence of a significant pressure gradient, a section with a logarithmic velocity profile survives. The EARSM-WL describes this effect quite adequately, while all other models predict an almost complete degeneracy of the logarithmic region (Figs. 8b, 9a). Note further that, in accordance with the EARSM-WL, the deviation of the function F from the constant value of 0.09 used in both base models occurring in the logarithmic region is not as significant as when the EARSM-CH is used (Fig. 10b).

The exactness of calculation of the kinetic energy of turbulence and its components $\overline{u'^2}$ and $\overline{v'^2}$ (see Figs. 9b, 10a) proves to be far from adequate even

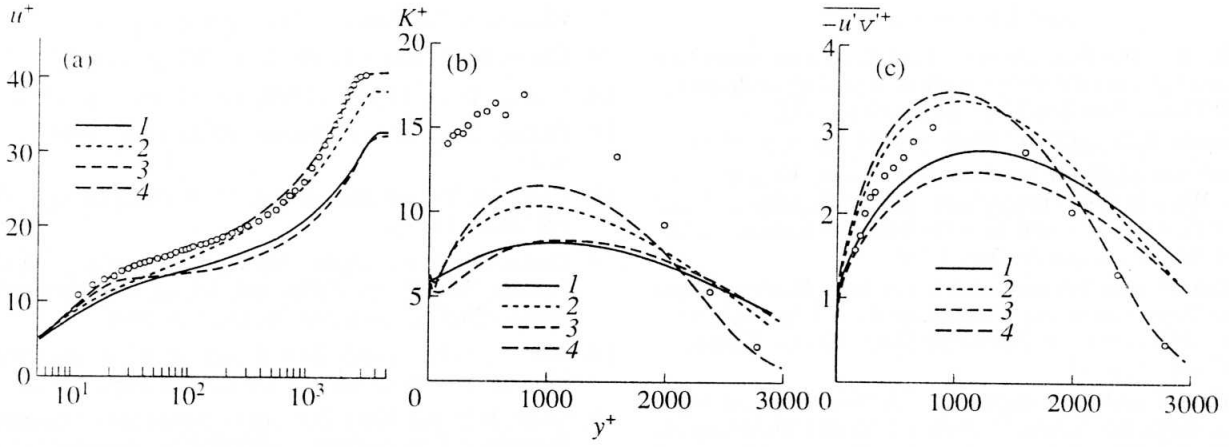

Fig. 9. Comparison of the results of calculation of the profile of (a) velocity, (b) kinetic energy of turbulence, and (c) tangential Reynolds stress in experiment 0141 for $x = 3.4$ m. Designations are the same as in Fig. 5.

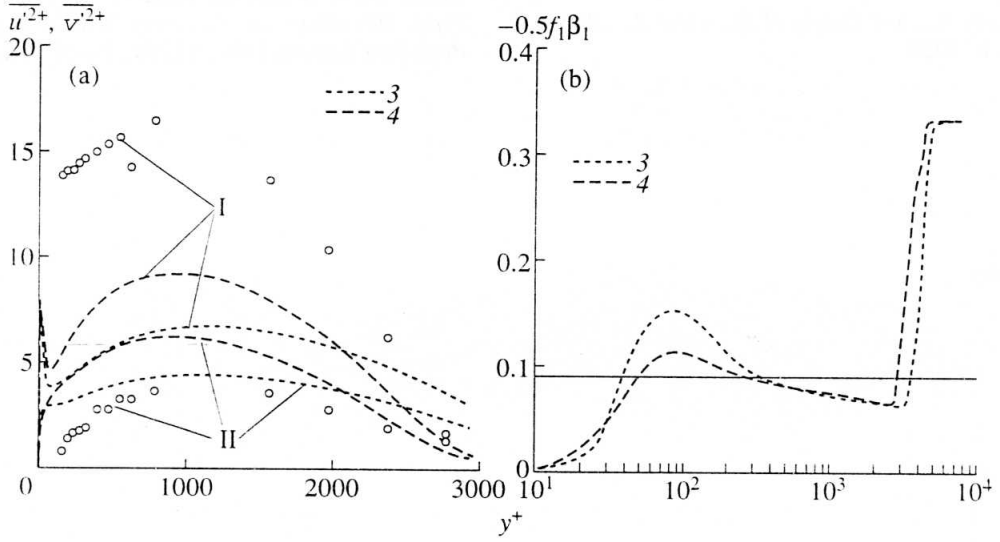

Fig. 10. The profiles of (a) the normal components of the Reynolds stress tensor and (b) the function $-0.5f_1\beta_1$ in experiment 0141 for $x = 3.4$ m, calculated using the models (*3*) EARSM-CH and (*4*) EARSM-WL. In Fig. 10a: I—$\overline{u'^2}$, II—$\overline{v'^2}$; the dots indicate the experiment.

when the best of the treated models, namely, EARSM-WL, is used. Although this does not affect the averaged flow parameters, which, as already noted, are fully defined by the quantity $\overline{u'v'}$, this defect of EARSM may prove important in calculating more complex flows in which an important part is played by all components of the Reynolds stress tensor.

CONCLUSION

The obtained results lead one to conclude that, as applied to the calculation of canonical wall turbulent boundary layers, the advantages of the EARSM over the traditional models of turbulence show up primarily when calculating the pulsation parameters of flow, although the EARSM fails to provide an adequately accurate prediction of the kinetic energy of turbulence and its individual components. It is significant that the accuracy of EARSM depends considerably on the choice of the base model and, from this standpoint, the K–ω model is superior to the K–ε model. Finally, the results of calculation of flow past a flat plate point to the need for a more thorough adjustment of the EARSM along with the base model.

ACKNOWLEDGMENTS

This study was supported by the Russian Foundation for Basic Research (grant 97-02-16492).

REFERENCES

1. Rodi, W., The Prediction of Free Turbulent Boundary Layers by Use of a Two Equation Model of Turbulence, *PhD Thesis*, London: Univ. of London, 1972.
2. Speziale, S.G., *AIAA J.*, 1997, vol. 35, no. 9, p. 1506.
3. *Prediction Methods for Turbulent Flows*, Kollman, W., Ed., Washington: Hemisphere, 1980. Translated under the title *Metody rascheta turbulentnykh techenii*, Kollman, W., Ed., Moscow: Mir, 1984.
4. Wallin, S. and Johansson, A.V., A New Explicit Algebraic Reynolds Stress Turbulence Model for 3D Flow, *Proc. 11th Symp. on Turbulent Shear Flows*, Grenoble, 1997, vol. 2, p. 13.
5. Wallin, S. and Johansson, A.V., A New Explicit Algebraic Reynolds Stress Turbulence Model Including an Improved Near-Wall Treatment, *Flow Modeling and Turbulence Measurements VI*, Chen, Shin, Lienau, and Kung, Eds., Rotterdam: Balkema, 1996.
6. Gatski, T.B. and Speziale, C.G., *J. Fluid Mech.*, 1993, vol. 254, p. 59.
7. Abid, R., Rumsey, C., and Gatski, T.B., *AIAA J.*, 1995, vol. 33, no. 11, p. 2026.
8. Kim, J., *J. Fluid Mech.*, 1989, vol. 285, p. 421.
9. Chien, K.-Y., *AIAA J.*, 1982, vol. 20, no. 1, p. 33.
10. Wilcox, D.C., *AIAA J.*, 1993, vol. 31, no. 8, p. 1414.
11. Durbin, P.A., *Theor. Comput. Fluid Dyn.*, 1991, no. 3, p. 1.
12. Catherall, D. and Mangler, K.W., *J. Fluid Mech.*, 1966, vol. 26, p. 163.
13. Garbaruk, A.V., Lapin, Yu.V., and Strelets, M.Kh., *Teplofiz. Vys. Temp.*, 1998, vol. 36, no. 4, p. 607 (*High Temp.* (Engl. transl.), vol. 36, no. 4, p. 583).
14. Menter, F.R., Zonal Two Equation K–ω Turbulence Models for Aerodynamic Flows, *AIAA Pap.*, 1993.
15. Coles, D.E. and Hirst, E.A., in *Computation of Turbulent Boundary Layers-1968: AFOSR-IFP Stanford Conf.*, Stanford Univ., Palo Alto, 1969, vol. 2.
16. Samuel, A.E. and Joubert, P.N., *J. Fluid Mech.*, 1974, vol. 66, p. 481.
17. Coles, D., A Model for Flow in the Viscous Sublayer, *Proc. Workshop on Coherent Structure of Turbulent Boundary Layers*, Lehigh Univ., Bethlehem, Pa., 1978.